Beyond scale separation in gyrokinetic turbulence

X. Garbet[1], Y. Sarazin[1], V. Grandgirard[1], G. Dif-Pradalier[1], G. Darmet[1], Ph. Ghendrih[1], P. Angelino[1], P. Bertrand[2], N. Besse[2], E. Gravier[2], P. Morel[2], E. Sonnendrücker[3], N. Crouseilles[3], J.-M. Dischler[4], G. Latu[4], E. Violard[4], M. Brunetti[5], S. Brunner[5], X. Lapillonne[5], T.-M. Tran[5], L. Villard[5] and M. Boulet[6]

[1] Association Euratom-CEA, CEA/DSM/DRFC Cadarache, France
[2] LPMIA -Université Henri Poincaré, Vandœuvre-lès-Nancy, France
[3] IRMA -Université de Strasbourg and INRIA Lorraine, France
[4] LSIIT -Université de Strasbourg, France
[5] CRPP Lausanne, Association EURATOM-Confédération Suisse, Switzerland
[6] CEA-DAM/DIF, Bruyères-le-Chatel, France, France

E-mail: xavier.garbet@cea.fr

Abstract
This paper presents the results obtained with a set of gyrokinetic codes based on a semi-Lagrangian scheme. Several physics issues are addressed, namely, the comparison between fluid and kinetic descriptions, the intermittent behaviour of flux driven turbulence and the role of large scale flows in toroidal ITG turbulence. The question of the initialization of full-F simulations is also discussed.

PACS numbers: 52.30.Gz, 52.35.Ra, 52.55.Fa

1. Introduction

Predicting turbulent transport in nearly collisionless fusion plasmas requires solving the gyrokinetic equations for all species coupled to the Maxwell equations. In spite of considerable progress, several pending issues remain. In particular, the choice of the method for solving the Vlasov equation is subject to intense debate. On the one hand, Eulerian codes have proved their efficiency, but are potentially subject to numerical dissipation, therefore requiring high order numerical schemes (see, e.g. [1]). On the other hand, Lagrangian codes (typically particle in cell codes) benefit from widespread experience, but may be affected by numerical noise. The latter problem can be cured by techniques of 'optimal loading' [2] and filtering. This paper presents an alternative method based on a semi-Lagrangian scheme [3] applied to gyrokinetics [4, 5]. This technique allows one to compute the full distribution function with moderate dissipation and has been assessed in several ways. Here, some physics issues are presented, namely, the intermittency in flux driven systems, the comparison between kinetic and fluid descriptions (including an alternative description based on a water bag model, and the dynamics of flows in full torus simulations of ion temperature gradient (ITG) turbulence.

2. Flux driven turbulence

Intermittency is addressed here in a system whose fluid counterpart is known to exhibit intermittency when the system is flux driven, namely, 2D interchange turbulence in the context of turbulence in the scrape-off layer of tokamaks. The kinetic version of this system is described by the drift-kinetic equation

$$\partial_t F + \boldsymbol{v}_E \cdot \nabla F + \boldsymbol{v}_D \cdot \nabla F = S, \qquad (1)$$

where F is a 3D distribution function, which depends on two spatial dimensions (x, y) (y is 2π periodical) and the energy E, S is a source term that depends on energy and position, $\boldsymbol{v}_E$ is the $E \times B$ electric drift velocity and $\boldsymbol{v}_D$ is the curvature drift velocity, which for this simplified system reads $\boldsymbol{v}_D = -E/eB_0R_0\boldsymbol{e}_y$, where e is the ion charge, B_0 the magnetic field and R_0 a characteristic curvature length (the major radius in a tokamak). Self-consistency is ensured by coupling the Vlasov equation equation (1) to the Poisson equation

$$\frac{n_{eq}e}{T_0}(\phi - \langle\phi\rangle) - \nabla_\perp \cdot \left(\frac{n_{eq}m_i}{eB_0^2}\nabla_\perp\phi\right) = \int dE F - n_{eq}, \quad (2)$$

where the bracket indicates an average over the periodic coordinate y, ϕ is the electric potential and n_{eq} is the
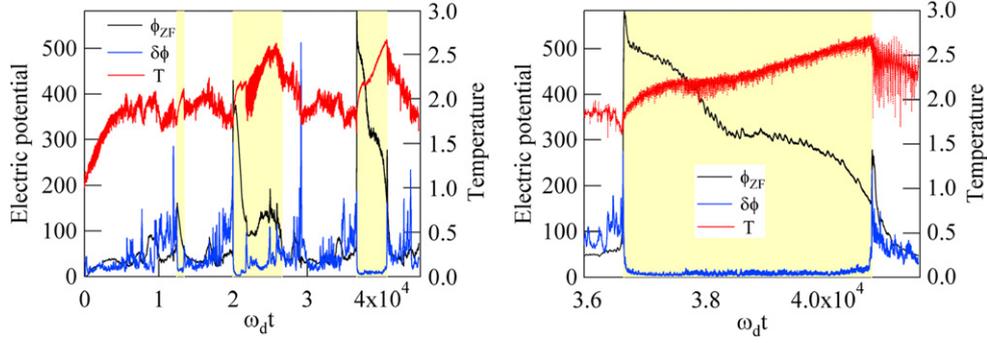
Figure 1. Left panel: time evolution of the volume averaged energy contents of zonal flows, electric potential fluctuations and central temperature T. Right panel: details of one relaxation (third time window in left panel).

density. Unless specified otherwise, the electron temperature is supposed to be constant, $T_e = T_0$. A trapped ion turbulence is also described by equations (1) and (2) when averaging the Vlasov equation over the fast cyclotron and bounce motions, up to an extra $E^{1/2}$ factor in expression (2) of the density [6]. The initial distribution function is a Maxwellian with prescribed density and temperatures, while fluctuations are set to zero.

The GYSELA code is usually run without sources. In this case boundary conditions are set such that the distribution function matches a Maxwellian with fixed density and temperature at both radial ends of the simulation box. However tokamak plasmas are flux driven, i.e. the temperature is controlled by a heat source and not by fixed values at the edges. Hence it is quite crucial to study systems where turbulence is flux driven. This has been done for a trapped ion turbulence (equations similar to equations (1) and (2), with an extra $E^{1/2}$ factor in the energy integration [6]) by implementing an energy dependent source term in the Vlasov equation (1). The source S is chosen of the form $S = S_0(x)(E/T - 1)$, where $S_0(x)$ is a Gaussian located close to $x = 0$. The dependence on energy $(E/T - 1)$ is such that the particle source is null while heat is injected in the system [7]. We single out the evolution of the volume average energies of zonal flow and fluctuating potential (without zonal flows), and the central temperature. An example of the rich dynamics of these three fields is reported in figure 1. When a large increase in the magnitude of the zonal flows occurs, the fluctuations are quenched and the core temperature builds up while the edge temperature decreases, in agreement with the usual picture for a transport barrier. In the first stage, the increase in the temperature gradient through the system takes place at the same time as the magnitude of the zonal flows decays away until an abrupt relaxation event takes place.

In the second stage, the relaxation governs a significant turbulence mixing during which the zonal flows are reduced, the radial temperature gradient flattens out and a large energy flux is transferred to the edge. The zonal flows build up again, then starting over such a predator–prey cycle. In such simulations the interplay between the zonal flows and the turbulent drift transport generates two distinct behaviours. In some cases there is a strong zonal flow overshoot that generates a transient transport barrier, while in other cases the zonal flows govern a saturation of the turbulent transport. This
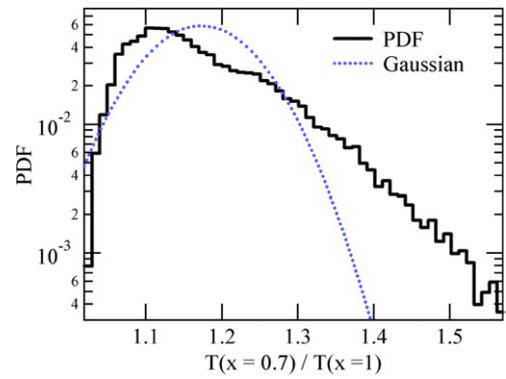

Figure 2. Probability distribution function of the temperature at $x = 0.3$ for flux driven kinetic interchange turbulence.

investigation of flux driven transport in a kinetic simulation confirms previous findings with fluid simulations for edge turbulence [8]. In particular the probability distribution function of temperature fluctuations is non-Gaussian (figure 2). Also it is found that a reduced description of the velocity space does not capture the right physics of an interchange turbulence described by equations (1) and (2). This motivates a detailed comparison between fluid and kinetic descriptions of interchange turbulence, presented in the next section.

3. Reduced 3D simulations: kinetic versus fluid descriptions

The fluid equations for interchange turbulence are obtained by computing the two first moments of equation (1), i.e.

$$\partial_t N + v_E \cdot \nabla N + v_D \cdot \nabla P = 0, \tag{3}$$

$$\partial_t P + v_E \cdot \nabla P + v_D \cdot \nabla Q = 0, \tag{4}$$

where N is the density, P the pressure and $Q = \int_0^{+\infty} dE\, E^2 F$ is the heat flux. For kinetic and fluid descriptions to match, an expression for Q, i.e. a closure, must be chosen. The simplest one consists of setting $Q = \Gamma PT$, where Γ is the adiabatic index (for a 2D system, a Maxwellian yields $\Gamma = 2$). To minimize the numerical errors, the same semi-Lagrangian scheme has been used to solve both the kinetic and the fluid equations. For the fluid case, this is done by solving the Vlasov equation for two energies $E_\pm$:

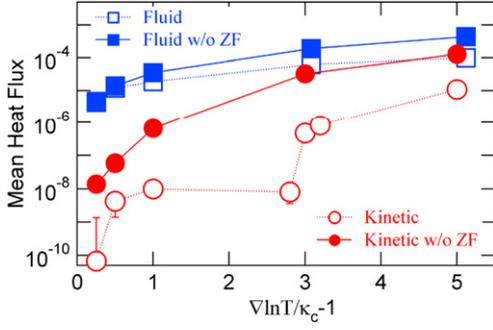$$\partial_t F_\pm + v_E \cdot \nabla F_\pm + v_{D\pm} \cdot \nabla F_\pm = 0, \tag{5}$$

Figure 3. Heat flux versus distance to the threshold κ_c comparing a 3D kinetic interchange turbulence equation (1) to the fluid equations (3) and (4) with diffusion added to match the instability threshold. The comparison is done with and without zonal flows.

Figure 4. Difference between the distribution function and the initial Maxwellian distribution for the kinetic interchange case.

where $v_{D\pm} = -E_{\pm}/eB_0R_0e_y$. The density and pressure are defined as $N = F_+ + F_-$ and $P = F_+E_+ + F_-E_-$. Using these definitions, the fluid equations equations (3) and (4) are recovered by summing the two equations (5) ruling $F_{\pm}$ with appropriate energy weights (1 for the density equation and $E_{\pm}$ for the pressure equation).

In this description, the heat flux is given by

$$Q = PT + 4(E_+ - E_-)^2 F_+ F_- / N. \qquad (6)$$

Hence it is found that the adiabatic index is close to one, $\Gamma = 1$, when E_+ is close to E_-. The advantage of this procedure is that both fluid and Vlasov equations are solved with the same solver, thus avoiding systematic errors due to the choice of numerical scheme. It is well known that the instability threshold derived from the fluid equations (3) and (4) (or equivalently equation (5)) differs from the kinetic value calculated from the Vlasov equation (1). To reduce this source of discrepancy, a diffusion coefficient has been added in equations (5), which is adjusted so that the kinetic and fluid instability linear growth rates nearly coincide.

The simulations show that the kinetic fluxes are well below the values calculated in the fluid approach, as shown in figure 3. This difference is usually explained by the dynamics of zonal flows [9] close to the instability threshold. However this is not the only explanation, as a difference persists when zonal flows are artificially suppressed (see figure 3). The remaining difference likely comes from wave/particle resonances, which are not well described by fluid equations. This can be seen from figure 4, which shows that even if the difference between the distribution function and the initial Maxwellian is small, the shapes are quite different in the energy space and cannot be described by a small number of moments [10]. It is stressed here that some enforcement towards a Maxwellian equilibrium comes from the boundary conditions at the edges of the simulation box (Maxwellian with prescribed density and temperature) and also from the initial state. One solution would be to add collisions to impose a relaxation towards a Maxwellian. Also it is possible that non-diffusive closure schemes, which have proved their efficiency in the past for δF codes [11, 12], would work [13]. An alternative solution, based on a water bag representation, is currently investigated and is presented in the next section.
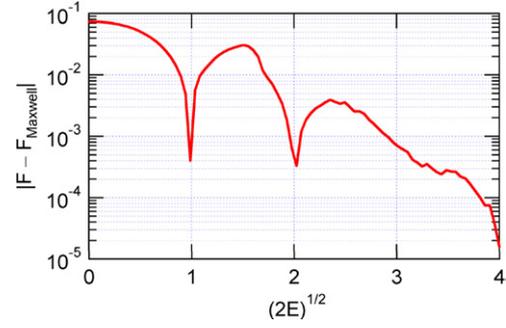
4. An alternative approach to kinetic versus fluid descriptions: the water bag model

The water bag model provides a bridge between kinetic and fluid descriptions. It offers an interesting alternative to the usual kinetic description, using the conservation property of the distribution function in the phase space. Accordingly, a discrete distribution function is assumed along the velocity direction, taking the form of a multi-step-like function. The water bag model was previously used only for non-magnetized plasmas because this model is well suited only for problems involving phase space with one velocity component. This model is applied for the first time to ITG modes in a cylinder. Slab ITG turbulence is described by the following set of equations:

$$\partial_t F + v_E \cdot \nabla F + v_{\parallel} \nabla_{\parallel} F - \frac{e}{m_i} \nabla_{\parallel} \phi \partial_{v_{\parallel}} F = 0, \qquad (7)$$

$$\frac{n_{eq}e}{T_0} (\phi - \langle\phi\rangle) - \nabla_{\perp} \cdot \left(\frac{n_{eq}m_i}{eB^2}\nabla_{\perp}\phi\right) = \int dv_{\parallel} J \cdot F - n_{eq}. \qquad (8)$$

The distribution function is now four-dimensional, with three space coordinates (the minor radius r, poloidal angle θ and coordinate along the cylinder axis), plus the velocity $v_{\parallel}$ along the magnetic field. In this case, the multi-step description of the distribution function reads

$$F(\boldsymbol{x}, v_{\parallel}, t) = \sum_{j=1}^{N} A_j \left\{ \Theta \left[v_{\parallel} + v_j (\boldsymbol{x}, t) \right] - \Theta \left[v_{\parallel} - v_j (\boldsymbol{x}, t) \right] \right\}, \qquad (9)$$

where N is the number of bags, A_j the height of the bag and Θ is a step function. Distribution function (9) is an exact solution of the Vlasov solution when the velocities $v_j(\boldsymbol{x}, t)$ evolve as follows:

$$\partial_t v_j + v_E \cdot \nabla v_j + v_j \nabla_{\parallel} v_j + \frac{e}{m_i} \nabla_{\parallel} \phi = 0. \qquad (10)$$

These are fluid-like equations, which offer an alternative to fluid equations with ad hoc closures. We note that the water bag representation is able to deal with a distribution function that is far from a Maxwellian. Nevertheless, as this is a rather new technique in the context of magnetized plasmas, the method has been tested first in a case where analytical results are known, namely, the linear stability of cylinder ITG modes for a
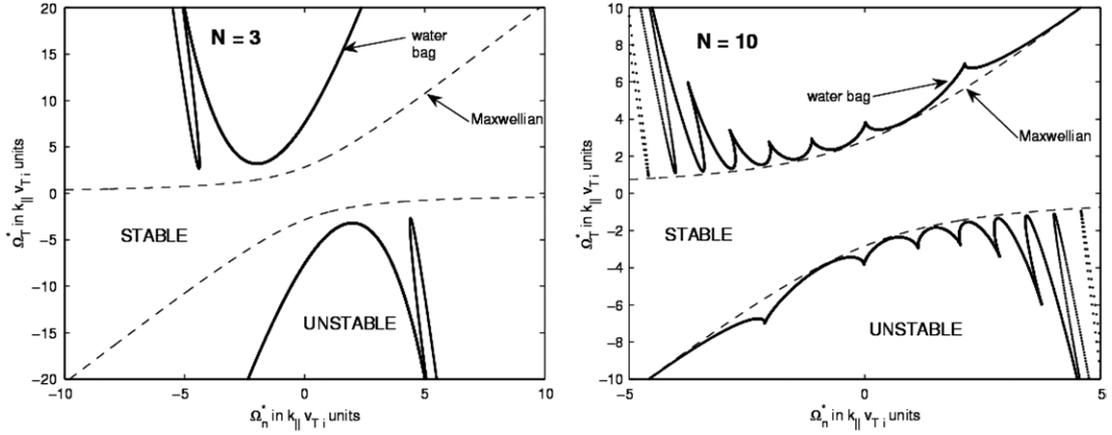
Figure 5. Instability diagram in the plane $\omega_T* = f(\omega_n*)$ for a multi-water bag distribution function and a Maxwellian.

Maxwellian background distribution function. Linearizing the set of equations (10), one gets the local dispersion relation of a drift-kinetic multi-water bag plasma for equal ion and electron temperatures, and hydrogenic species:

$$\varepsilon(\omega) = 1 - \sum_{j=1}^{N} \alpha_j \frac{k_\parallel^2 c_s^2 - \omega \omega_j^*}{\omega^2 - k_\parallel^2 a_j^2} = 0, \quad (11)$$

where a_j is the initial ('equilibrium') parallel velocity v_j, $c_s = (T_{eq}/m_i)^{1/2}$ is the thermal velocity, $\alpha_j = n_{eq,j}/n_{eq}$ is related to the density of the jth bag $n_{eq,j} = 2a_j A_j$ and the diamagnetic frequency for each bag is defined as

$$\omega_j^* = \frac{k_\theta T_{eq}}{eB} \frac{\partial_r n_{eq,j}}{n_{eq,j}}. \quad (12)$$

Finding the complex roots of equation (11) provides the linear growth rate, whose existence and value essentially depend on the values of the density and temperature diamagnetic frequencies $\omega_n^* = k_\theta T_{eq} \partial_r \ln(n_{eq})/eB$ and $\omega_T^* = k_\theta T_{eq} \partial_r \ln(T_{eq})/eB$. The one bag case can be shown to be equivalent to the adiabatic fluid description, without any instability, and a constant ratio between temperature and density gradients ($L_n/L_T = 2$). The instability threshold for ITG instability is found to be close to the results obtained from continuous Maxwellian distribution function when $N = 10$, except for large density gradients (see figure 5) [14]. The method remains to be tested in the non linear regime, first for the interchange turbulence described in section 2, second in the 4D slab geometry where it will be compared with a 4D version of the GYSELA code [5, 15] and finally to the full 5D toroidal case.

5. Global non-perturbative simulations of toroidal ITG turbulence

The GYSELA code has been upgraded to run 5D simulations of toroidal ITG turbulence [16]. The codes solves the gyrokinetic equation

$$\partial_t F + \mathbf{v}_E \cdot \nabla F + \mathbf{v}_D \cdot \nabla F + v_\parallel \nabla_\parallel F + \dot{v}_\parallel \partial_{v_\parallel} F = 0, \quad (13)$$

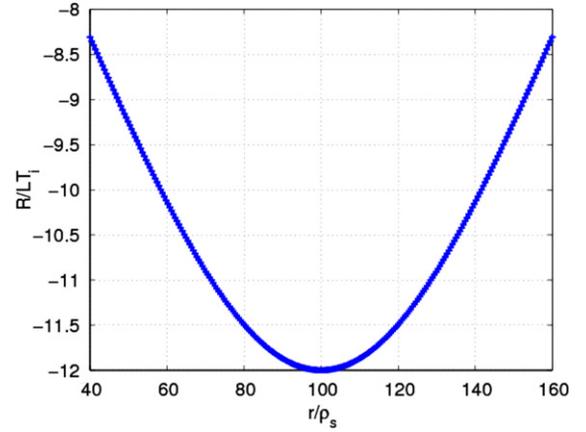**Figure 6.** Initial profile of R/L_{Ti} in GYSELA runs.

where

$$\mathbf{v}_E = \frac{\mathbf{B} \times \nabla(J \cdot \phi)}{B^2}; \qquad \mathbf{v}_D = \frac{m_i v_\parallel^2}{eB} \left(\frac{\mathbf{B}}{B} \times \frac{\mathbf{N}}{R} \right)$$
$$+ \frac{\mu}{e} \left(\frac{\mathbf{B}}{B} \times \frac{\nabla B}{B} \right), \quad (14)$$

$$m_i \dot{v}_\parallel = - \left[\frac{\mathbf{B}}{B} + \frac{m_i v_\parallel}{eB} \left(\frac{\mathbf{B}}{B} \times \frac{\mathbf{N}}{R} \right) \right] \cdot (\mu \nabla B + e \nabla J.\phi), \quad (15)$$

where $\mathbf{N}/R$ is the field line curvature. The Poisson equation reads

$$\frac{n_{eq}e}{T_0}(\phi - \langle \phi \rangle) - \nabla_\perp \cdot \left(\frac{n_{eq}m_i}{eB^2} \nabla_\perp \phi \right)$$
$$= \int B d\mu dv_\parallel J \cdot F - n_{eq}, \quad (16)$$

where J is the gyroaverage operator (multiplication by $J_0(k_\perp \rho_c)$ in Fourier space, ρ_c is the gyroradius—the present implementation of this operator is based on a Padé representation of the Bessel function J_0). The code uses a simplified geometry based on a set of circular centred magnetic surfaces with a magnetic field $\mathbf{B} = B_0 R_0/R(\mathbf{e}_\varphi + r/q R_0 \mathbf{e}_\theta)$ and $R = R_0 + r \cos(\theta)$. No source is added in this version of the code. Boundary conditions are such that the distribution function matches a Maxwellian with fixed density and temperature at both radial ends of the simulation domain.
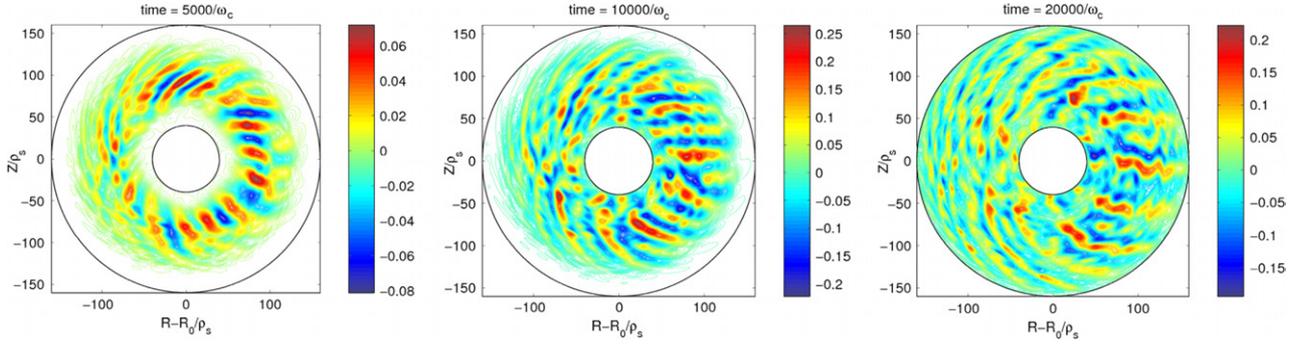
Figure 7. Poloidal cross section of the electric potential for an ITG turbulence simulation when zonal flows are artificially suppressed ($\rho_* = 0.005$).

The parameters of the simulation correspond to the Cyclone base case [9] with a gyroradius normalized to the plasma size ρ_* equal to 0.005.

Several numerical tests have been done to check the accuracy when solving the Vlasov equation, in particular regarding the conservation of motion invariants [16]. Also the linear growth rates agree well with the expected values, and the $n = 0$, $m = 0$ component of the electric potential, labelled ϕ_{00}, evolves as expected. Namely, it decays while emitting geodesic acoustic modes, with a damping rate that agrees with the value calculated by Sugama and Watanabe [17]. The flow ultimately relaxes towards a non-zero residual value, as prescribed by Rosenbluth and Hinton [18]. In the following the non linear simulations are initiated with a quasi-parabolic profile such that $R/L_{\mathrm{Ti}} = 12$ at mid-radius, and $T_{\mathrm{e}} = T_{\mathrm{i}}$ (figure 6). No source is added, so that the temperature gradient decays slowly during the simulation.

For an initial distribution function is a Maxwellian of the form

$$F_{\mathrm{eq}}(r, E) = \frac{n_{\mathrm{eq}}(r)}{\left[2\pi m T_{\mathrm{eq}}(r)\right]^{3/2}} \exp\left\{-\frac{E}{T_{\mathrm{eq}}(r)}\right\}, \qquad (17)$$

where $E = m v_\parallel^2/2 + \mu B$, and in the case where ϕ_{00} is artificially suppressed, a standard shearless ITG turbulence develops, as shown in figure 7.

However when ϕ_{00} is self-consistently calculated, large scale steady flows appear, which prevent the onset of turbulence (see figure 8). This is a consequence of the equilibrium distribution function not being a function of the motion invariants. If the distribution function is a function of the minor radius instead of the canonical toroidal moment, no parallel flow exists initially to balance the charge separation associated with the ion curvature drift. Hence a polarization drift appears to ensure the charge balance. Parallel flows develop in a second stage, but the shear flow is too strong to allow a growth of turbulence [19, 20]. In some cases, turbulence ultimately develops but on a slow time scale. It is in fact much safer to ensure the charge balance by allowing the development of parallel flows, in particular ($n = 0$, $m = 1$) components (Pfirsch–Schlüter effect).

A similar problem was already mentioned by Idomura *et al* [21] and by Angelino *et al* [22]. It is cured by prescribing an equilibrium distribution function that is canonical, i.e. a function of motion invariants. The choice here is the same
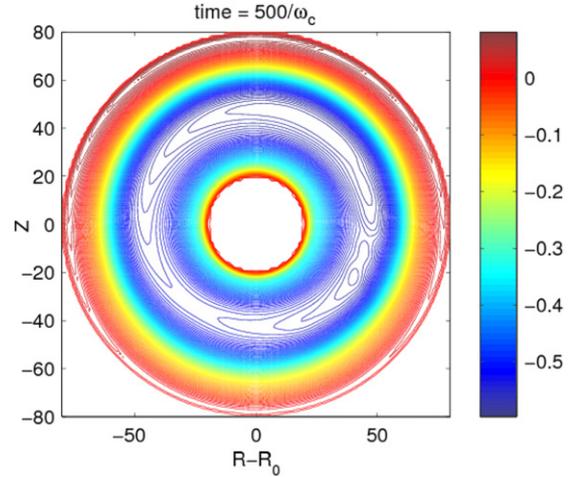

Figure 8. Poloidal cross section of the electric potential for an ITG turbulence simulation when zonal flows are included and non-canonical initial distribution function ($\rho_* = 0.005$).

as the one proposed in the [22], that is a distribution function of form (17), with the minor radius r replaced by the motion invariant $\bar{r}$ defined as

$$\bar{r} = r_0 - \frac{q_0}{r_0} \int_{r_0}^{r} \frac{r\,\mathrm{d}r}{q} + \frac{q_0}{r_0} \frac{m}{eB_0} \left(R v_\parallel - R_0 \bar{v}_\parallel\right), \qquad (18)$$

where

$$\bar{v}_\parallel = sign\left(v_\parallel\right) \left[\frac{2}{m}\left(E - \mu B_{\mathrm{m}}\right)\right]^{1/2} \Theta\left(E - \mu B_{\mathrm{m}}\right) \qquad (19)$$

and Θ is a step function, B_{m} is the maximum of magnetic field in the whole box (all quantities with a label 0 are defined at half-radius of the simulation box). With this prescription, the average parallel velocity and electric potential evolve towards steady values. The final state is turbulent, and the level of fluctuations $e(\phi - \phi_{\mathrm{eq}})/T_{\mathrm{eq}}$ lies in the expected range (figure 9) (ϕ_{eq} is the time average of ϕ_{00}). In this configuration the corresponding $E \times B$ shear rate is small enough not to affect the turbulent transport. When comparing figures 7 and 9, it appears that the radial size of vortices is reduced by the shearing effect of zonal flows, as expected [23]. Also the thermal flux is in the right order of magnitude when compared with the Cyclone curve giving the flux versus the normalized temperature gradient (figure 10) [9]. The simulation shown in
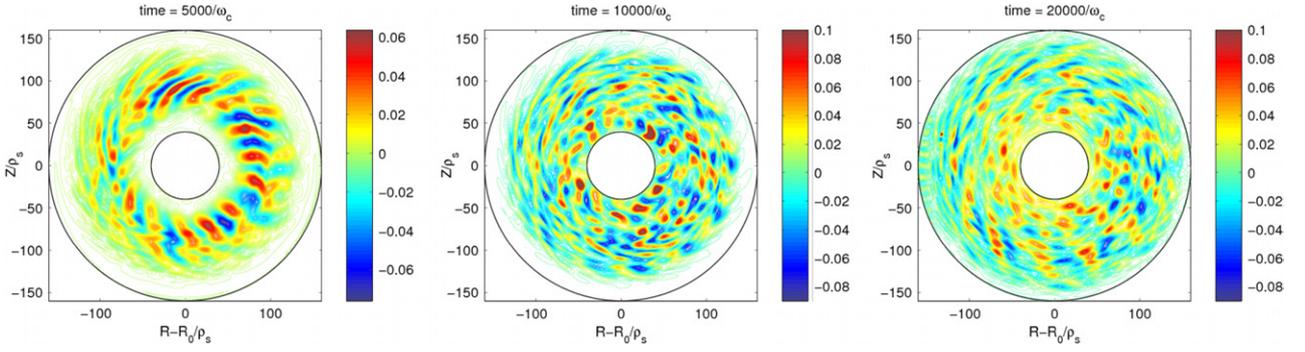
Figure 9. Poloidal cross section of the electric potential fluctuations $e(\phi - \phi_{eq})/T_{eq}$ for an ITG turbulence with zonal flows included and an initial distribution function that is canonical ($\rho_* = 0.005$).
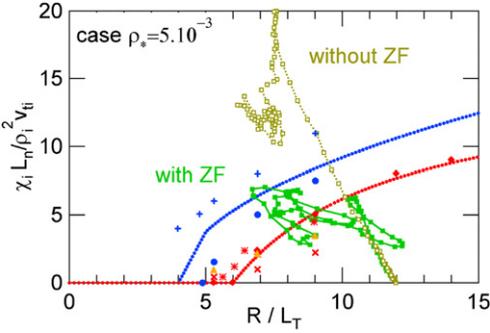

Figure 10. Time evolution of the calculated thermal flux at mid-radius for the simulations with (full squares, green) and without (open squares, yellow) zonal flows (ZF) corresponding to figure 7 (without ZF) and 9 (with ZF). The fluxes are compared with the Cyclone results for fluid (crosses and circles) and kinetic (diamonds and stars) simulations [9].

figure 9 was run on the BULL-TERA10 supercomputer, which is a cluster of 9968 processors Novascale 5160 that offers a 60 Teraflops computing capability [24]. The number of mesh points is $(r, \theta, \varphi, v_\parallel, \mu) = (256, 256, 64, 32, 8)$ (full torus simulation), and the time step is $\Omega_c \Delta t = 5$ for a normalized gyroradius $\rho_* = 0.005$. The CPU time needed to reach $\Omega_c \Delta t = 20\,000$ is 70 h on 64 processors.

We note that the difference between $\bar{r}$ and r is of the order of ρ_s. Hence this procedure should not be necessary any more for low enough values of ρ_*. Nevertheless it sounds safer to choose an initial distribution function that is solution of the Vlasov equation, i.e. $[H_{eq}, F_{eq}] = 0$.

Regarding this question, it appears that the prescription equations (17) and (18) belongs to a larger class of equilibrium distribution functions [25], defined for a general magnetic field $\boldsymbol{B} = I(\psi)\nabla\varphi + \nabla\psi \times \nabla\varphi$ as

$$F_{eq}(\bar{\psi}, E, w_\parallel) = \frac{n_{eq} \exp\left(e\phi_{eq}/T_{eq}\right)}{\left[2\pi m T_{eq}\right]^{3/2}} \exp\left\{-\frac{H}{T_{eq}}\right\}$$
$$\times \left\{1 + \frac{m\bar{v}_\parallel W_{\parallel eq}}{T_{eq}}\right\}, \tag{20}$$

where n_{eq}, T_{eq} and $W_{\parallel eq}$, are functions of the motion invariant $\bar{\psi} = \psi + mIv_\parallel/eB$, $H = mv_\parallel^2/2 + \mu B + e\phi_{eq}$ is the energy and $\bar{v}_\parallel$ is the motion invariant defined by equation (19), with a slightly different definition of B_m

$$B_m = B\left(\bar{\psi}, \theta = \pi\right)(E - \mu B_{max}). \tag{21}$$

Developing equation (20) at first order in ρ_* and calculating the 2nd moment yield the fluid velocity

$$\boldsymbol{V} = W_{\parallel eq}(\psi)\frac{\boldsymbol{B}}{B_{max}(\psi)} + \left(\frac{d\phi_{eq}}{d\psi} + \frac{1}{n_{eq}e}\frac{dp_{eq}}{d\psi}\right)R^2\nabla\varphi. \tag{22}$$

This expression is fully consistent with the usual prescription for the equilibrium velocity in a tokamak and satisfies the force balance equation $\boldsymbol{E} + \boldsymbol{V} \times \boldsymbol{B} - \nabla p/ne = 0$. In a collisionless code, the choice of the function $W_{\parallel eq}$ is arbitrary. The choice equation (20) minimizes the mean parallel velocity, as mentioned in [22]. Adding collisions would lead to a different result as the neoclassical viscous damping prescribes a value of $W_{\parallel eq}$ that usually corresponds to a finite parallel velocity. Hence the choice of the initial distribution function is intimately related to the structure of the initial mean flow, which can be chosen by prescribing the values of ϕ_{eq} and $W_{\parallel eq}$.

6. Conclusion

A sequence of gyrokinetic codes with increasing dimensionality and based on a semi-Lagrangian scheme has been developed and used to clarify several physics issues related to the interplay between flows and turbulence and the scale separation assumption. Flux driven interchange turbulence has been simulated. As in previous fluid flux driven simulations, strong intermittency is observed. It is related to abrupt relaxations of the temperature profile, correlated with fast events in the zonal flow and fluctuation dynamics. Also turbulent fluxes for a 3D interchange turbulence are found to be different when using fluid or kinetic equations. This discrepancy is partially due to the different behaviour of zonal flows. Moreover the shape of the distribution function in the energy space is found to differ significantly from a Maxwellian, suggesting that part of the difference is due to resonant wave/particle interaction. An alternative to fluid description that describes kinetic effects, the water bag representation, has been studied. It is shown to reproduce correctly the kinetic linear growth rate and frequencies with a limited amount of bags. It remains, however, to be tested in the non-linear regime. Finally a 5D version of the GYSELA code has been developed to study toroidal ITG turbulence. The linear growth rates agree with the values expected for the Cyclone base case and zonal flows behave as expected. The choice of the initial distribution function is

crucial for the non-linear stage. The best option is to choose a function of motion invariants to avoid the development of spurious large scale flows, which may prevent the development of turbulence. Once the distribution function is properly initialized, the simulations produce turbulent heat fluxes in the expected range.

References

[1] Candy J. and Waltz R.E. 2003 *J. Comput. Phys.* **186** 545
[2] Hatzky R. *et al* 2002 *Phys. Plasmas* **9** 898
[3] Sonnendrücker E., Roche J., Bertrand P. and Ghizzo A. 1999 *J. Comput. Phys.* **149** 201
[4] Brunetti M., Grandgirard V., Sauter O., Vaclavik J. and Villard L. 2004 *Comput. Phys. Commun.* **163** 1
[5] Grandgirard V. *et al* 2006 *J. Comput. Phys.* **217** 395
[6] Depret G. *et al* 2000 *Plasma Phys. Control. Fusion* **42** 949
[7] Darmet G. *et al* 2007 Intermittency in flux driven kinetic simulations of trapped ion turbulence *Proc. Vlasovia Conf. (2006) Commun. Nonlinear Sci. Numer. Simul.* at press
[8] Ghendrih Ph. *et al* 2005 *J. Nucl. Mater.* **337–339** 347
[9] Dimits A.M. *et al* 2000 *Phys. Plasmas* **7** 969
[10] Sarazin Y. *et al* 2005 *Plasma Phys. Control. Fusion* **47** 1817
Sarazin Y. *et al* 2006 *Plasma Phys. Control. Fusion* **48** B179
[11] Hammet G.W. and Perkins F.W. 1990 *Phys. Rev. Lett.* **64** 3022
[12] Waltz R.E. *et al* 1997 *Phys. Plasmas* **4** 2482
[13] Fleurence E. *et al* 2006 Entropy production rate as a constraint for collisionless fluid closures *Joint Varenna-Lausanne Int. Workshop on the Theory of Fusion Plasmas AIP Conf. Proc.* **871** 336
[14] Morel P. *et al* The Water Bag model for gyrokinetic simulations *Phys. Plasmas.* submitted
[15] Sarazin Y. *et al* 2006 *Phys. Plasmas* **13** 092307
[16] Grandgirard V. *et al* 2006 *Proc. Int. Theory Conf. Theory of Fusion Plasmas (Varenna, 2006) AIP Conf. Proc.* **871** 100
[17] Sugama H. and Watanabe T.-H. 2006 *Phys. Plasmas* **13** 012501
[18] Rosenbluth M.N. and Hinton F.L. 1998 *Phys. Rev. Lett.* **80** 724
[19] Biglari H., Diamond P.H. and Terry P.W. 1990 *Phys. Fluids* B **2** 1
[20] Waltz R.E., Kerbel G.D. and Milovitch J. 1994 *Phys. Plasmas* **1** 2229
[21] Idomura Y. *et al* 2003 *Nucl. Fusion* **43** 234
[22] Angelino P. *et al* 2006 *Phys. Plasmas* **13** 052304
[23] Lin Z. *et al* 1998 *Science* **281** 1835
[24] J.-L. Lahaie 2006, private communication
[25] Dif-Pradalier G. *et al* 2007 Defining an equilibrium state in global full-f gyrokinetic models *Proc. Vlasovia Conf. (2006) Commun. Nonlinear Sci. Numer. Simul.* at press